Sources and Sinks of Anthropogenic CO_2:

Integrated Assessment Using Biogeochemical Modeling and Inversion of Atmospheric Tracer Transport

Final Report

Jorge Sarmiento, and Song-Miao Fan

Atmospheric & Oceanic Sciences Program, Princeton University

Princeton, New Jersey 08544

Summary: With support from the NSF Methods and Models for Integrated Assessment initiative, we have developed an isotopic method for direct calculation of the sources and sinks of atmospheric CO_2 through inverse modeling of observational data using a GFDL global three-dimensional tracer transport model. We modeled the distribution of $\delta^{13}C$ ratios in the atmosphere observed during 1993-1995, and estimated the terrestrial net ecosystem production for three geographical regions. The land biota in North America and Eurasia was found to be absorbing CO_2, at a rate of about 2 GtC yr^{-1}, while that in Tropics and the Southern Hemisphere were found to be releasing CO_2 during this three-year period.

1. Introduction

The global carbon cycle involves multiple components of the Earth system, including the atmosphere, the ocean, the terrestrial biosphere, and anthropogenic emissions. We proposed an integrated program to develop methods to assess the current carbon budget, and at the same time to build the tools to allow a mechanistic study of the processes involved so that realistic prediction of changes to these processes may become more feasible. In particular, we proposed to develop an isotopic inverse

method for the estimation of terrestrial carbon sources and sinks over the globe as a part of the integrated program.

The following tasks have been completed:

(a) We carried out forward model simulations of carbon isotopes in the atmosphere caused by fossil fuel emissions, annual average air-sea exchange fluxes, and seasonal terrestrial net primary production (NPP) and heterotrophic respiration (RESP).

(b) We developed an isotopic inverse method, and evaluated the inverse method using "synthetic" data generated by a separate atmospheric model. The evaluation provides a critical assessment of transport errors inherent in our inverse estimates.

(c) Terrestrial net carbon fluxes during 1993-1995 were estimated using the inverse method for North America, Eurasia, Tropics and the Southern Hemisphere.

We will document in this report (1) the basics of carbon isotope biogeochemistry, (2) forward modeling of carbon isotopes in the atmosphere using a global chemical transport model, (3) an inverse method for carbon isotopic ratios, and (4) inverse estimates of terrestrial carbon sources and sinks.

2. The Isotopic Method

Measurements of carbon isotopic ratios are often presented in the 'delta notation', $\delta^{13}C$, as follows:

$$\delta^{13}C = \frac{R - R_{PDB}}{R_{PDB}} \times 1000$$

where R is $^{13}C/^{12}C$ ratio, and R_{PDB} = 0.0112372 is the ratio found in Pee Dee Belemnite calcite and the reference ratio used internationally for reporting measurements. Typical values of $\delta^{13}C$ are listed in Table 1 for various carbon reservoirs.

Table 1. Typical isotopic ratios of carbon reservoirs

Carbon reservoirs	$\delta^{13}C$ (‰)
Atmosphere	-6.4 around 1740, -7.8 around 1990
Ocean	~1.6 surface ocean (c. 1990), ~2.1 deep sea
Land biota	-25 for C_3 forests, -12 for C_4 pastures
Fossil fuel	-24 for coal, -44 for natrual gas, -26 to -30 for crude oil
Cement production	0.0
Mean fossil CO_2	-24.1 c. 1860, -28.2 c. 1980, -28.4 c. 1990

We can use the $\delta^{13}C$ ratio of CO_2 to distinguish terrestrial from marine fluxes. Because plants discriminate against ^{13}C in photosynthetic carbon assimilation (see Table 2). By contrast, the kinetic fractionation of carbon isotopes during the transfer from the atmosphere to the ocean is small (-2‰); atmospheric $\delta^{13}C$ is nearly unchanged by the uptake of CO_2 into the surface oceans. The difference of $\delta^{13}C$ between the atmosphere and seawater (~9‰) is mainly due to the kinetic fractionation during the transfer from the ocean back to the atmosphere (-11‰).

The atmosphere is near equilibrium with the surface ocean with regard to the isotopic composition of CO_2. However, a small isotopic dis-equilibrium has resulted from anthropogenic perturbations to the global carbon cycle since the Industrial Revolution. Anthropogenic CO_2 from fossil fuel consumption and deforestation sources is depleted in ^{13}C, causing atmospheric CO_2 and disolved inorganic carbon in seawater to become isotopically lighter (the ratio of $^{13}C/^{12}C$ decreasing) with time. This trend of isotopic ratio is called the "Suess effect". The oceanic Suess effect lags behind

that in the atmosphere due to a relatively long air-sea equilibration time (years) for the isotopic compositions compared to the equilibration time for CO_2 concentrations (months). As a result, an isotopic dis-equilibrium develops between the atmosphere and the global ocean.

Table 2. Typical isotopic fractionation

Processes	*Fractionation* (‰)
Air-C_3 plants	-20
Air-C_4 plants	-4
Air-sea	-2
Sea-air	-10.2

An isotopic dis-equilibrium has similarly developed between soil carbon and atmospheric CO_2, as old soil carbon was assimilated one to hundreds of years ago when the carbon isotopes ratio in the atmosphere was different than at the present time. Because of the presence of the isotopic dis-equilibria, atmospheric $\delta^{13}C$ is changed (increased) even when terrestrial respiration balances terrestrial net primary production and CO_2 evasion from sea to air balances CO_2 invasion from air to sea over annual cycles.

2. Modeling of isotopic ratios

Our goal is to determine the contribution of surface carbon fluxes that will best predict observations of the spatial structure of CO_2 and $\delta^{13}C$ in the atmosphere. We define the spatial structure in reference to South Pole observations (or model results) in **January** of each year, and denote

$$\Delta C = C - C_{SPO} \qquad \text{for } CO_2,$$

$$\Delta^{12}C = {}^{12}C - {}^{12}C_{SPO} \qquad \text{for } {}^{12}CO_2, \text{ and}$$

$$\Delta^{13}C = {}^{13}C - {}^{13}C_{SPO} \qquad \text{for } {}^{13}CO_2.$$

Because the South Pole Observatory (SPO) is remote from carbon sources and sinks, monthly measurements can be obtained from four weekly flask samples with minimal biases due to local and synoptic variations. Local sources represent subgrid variations, and are not resolved in the global model. Changes in the isotopic ratios are given by:

$$\Delta\delta^{13}C = \delta^{13}C - \delta^{13}C_{SPO} = \frac{\Delta R}{R_{PDB}} \times 1000$$

$$\Delta\delta^{13}C = \frac{1000}{R_{PDB}} \Delta\left[\frac{{}^{13}C}{{}^{12}C}\right] = \frac{1000}{R_{PDB}}\left(\frac{\Delta^{13}C}{{}^{12}C} - R_{SPO}\frac{\Delta^{12}C}{{}^{12}C}\right)$$

$$\Delta\delta^{13}C = \frac{1000}{R_{PDB}}\left(\frac{(1+R_{SPO})\Delta^{13}C}{C} - R_{SPO}\frac{\Delta C}{C}\right)(1+R)$$

$$\Delta\delta^{13}C \approx \frac{1000}{R_{PDB}}\left(\frac{(1+R_{SPO})\Delta^{13}C}{C_{SPO}} - R_{SPO}\frac{\Delta C}{C_{SPO}}\right)\left(1-\frac{\Delta C}{C_{SPO}}\right)(1+R)$$

Rearranging above equation, and neglecting the near identity factors (1+R) and (1-$\Delta C/C_{SPO}$), we obtain:

$$C_{SPO} \bullet \Delta\delta^{13}C \approx \frac{1000}{R_{PDB}}\left((1+R_{SPO})\Delta^{13}C - R_{SPO}\Delta C\right)$$

Given surface fluxes of CO_2 and $^{13}CO_2$, we use atmospheric transport models to predict the spatial and temporal structures of ΔC and $\Delta^{13}C$, and then use above equation to compute $\Delta\delta^{13}C$.

We simulated in the GFDL Global Chemical Transport Model (GCTM) atmospheric CO_2 and $\delta^{13}C$ caused by fossil fuel emissions, air-sea exchanges, and seasonal biotic sources and sinks on land. The model specifies fossil fuel emissions based on the estimates of Andres et al. (1995), and prescribes oceanic fluxes based on an aseasonal (annual mean biology) ocean model (Murnane et al., 1998). Figure 1 shows the isotopic ratios of fossil carbon released by each nation. For the United States, we use isotopic ratios estimated for each state and for each month (Figures 2a and 2b), provided to us by Robert Andres at the University of Alaska. Spatial and temporal variations in the isotopic ratios of fossil carbon reflect changes in the types of fuel consumed, with natural gas being the most depleted in ^{13}C and coal the least depleted (see Table 1).

The spatial and temporal patterns for the terrestrial biospheric carbon fluxes are taken from the Carnegie, Ames, and Stanford Approach (CASA) biospheric model (Potter et. al., 1993). The isotopic fractionation coefficients vary significantly from boreal forest to tropical savanna (Neil Suits, Colorado State University). However, we did not have the terrestrial model results when the isotopic inverse model was constructed; we assumed uniform isotopic fractionations for three large regions (Figure 3). It can be shown for a terrestrial source of uniform isotopic ratios that the atmospheric response is given by:

$$C_{SPO}\Delta\delta^{13}C = a(x,t)\left(\delta^{13}C_{leaf} - \delta^{13}C_{SPO}\right)F$$

where *a(x,t)* is atmospheric response at location *x* and at time t to a source of 1 GtC yr^{-1} , and *F* is a flux multiple. Let $\mathbf{D = C_{spo} \bullet \Delta\delta^{13}C}$ (unit: ppm‰). We then have:

where ***i*** = Eurasia, North America, and Tropics+SH, and

$$D_{mod\ el} = D_{fossil} + D_{ocean} + \sum_i (D_{i,resp} - D_{i,npp})$$

$$D_{i,resp} = [iso\_RESP]_i \bullet a_{i,resp}(x,t)$$

$$D_{i,npp} = [iso\_NPP]_i \bullet a_{i,npp}(x,t)$$

The *isotopic fluxes* are related to carbon fluxes by:

$$[iso\_RESP] = (\delta^{13}C_{SOM} - \delta^{13}C_{SPO}) \bullet [RESP] \quad \text{and}$$

$$[iso\_NPP] = (\delta^{13}C_{leaf} - \delta^{13}C_{SPO}) \bullet [NPP]$$

and are in units of ‰GtC yr^{-1} , $a_{i,resp}(\mathbf{x},t)$ and $a_{i,npp}(\mathbf{x},t)$ are predicted CO_2 for CASA model respiration and net primary production (normalized to 1 GtC yr^{-1}), respectively, and are in units of ppm/(GtC yr^{-1})

The inverse model substitutes D_{model} with observations D_{obs}, and then solves

$$D_{obs} = D_{fossil} + D_{ocean} + \sum_i \left(a_{i,resp}(x,t)[iso\_RESP]_i - a_{i,npp}(x,t)[iso\_NPP]_i \right)$$

for the isotopic fluxes [iso_RESP] and [iso_NPP] caused by terrestrial net primary production (NPP) and respiration (RESP) for three land regions: North America (north of 15°N), Eurasia and North Africa (north of 24°N), and Tropics and Southern Hemisphere (Figure 3). We chose to solve for three regions because we are limited by the spatial coverage of observations (Gloor et al., 1999). We used the inverse model to

estimate CO_2 fluxes and isotopic fluxes that give best fit to the the spatial gradients, seasonal variations, and annual trends in atmospheric CO_2 and $\delta^{13}C$ observed at 70 CMDL sampling sites during a three year period between 1993-1995 (Pieter Tans, CMDL; Jim White, University of Colorado INSTAAR). The inverse model uses a robust estimation method that is insensitive to outliers, and uses the "downhill simplex minimization" algorithm (Press et al., 1998).

3. Model Results

Figure 4 shows the distribution of zonal average atmospheric $\delta^{13}C$ caused by fossil emissions and oceanic fluxes. Fossil carbon fluxes cause atmospheric $\delta^{13}C$ to be more negative in the Northern Hemisphere than in the Southern Hemisphere. Oceanic fluxes increase atmospheric $\delta^{13}C$ in the tropics and decrease atmospheric $\delta^{13}C$ in the mid-high latitudes, but do not cause a large north-south gradient.

In order to evaluate the simple inverse model, we used another GFDL atmospheric model (SKYHI) to generate synthetic "data" with the same fossil fuel and oceanic carbon fluxes as used in the GCTM model, and with presumed annual net terrestrial fluxes super-imposed on the CASA model NPP and RESP fluxes. The presumed net terrestrial fluxes are uniformly propotrtional to NPP in each grid cell and in each month. The fluxes estimated by the inversion are shown in Tables 3a-d for four sets of synthetic "data" generated in SKYHI using different presumed fluxes. The global ocean uptake was also estimated in the test inversions, while its spatial distribution was specified. Table 3a shows that the estimated carbon fluxes are close to zero, in good agreement with the presumed fluxes. This is an improvement over inversions based on annual average data where the "rectification effect" causes erroneous compensating fluxes of order 0.7 GtC/year in Eurasia and North America. Table 3b shows that the differences in fossil CO_2 gradient between the two transport models cause erroneous terrestrial uptake in North America and Eurasia, because higher fossil CO_2 is simulated in the

Northern Hemisphere in GCTM than in SKYHI. A presumed terrestrial carbon sink in North America is well estimated by the inverse model (Table 3c). However, the differences between SKYHI and GCTM cause a presumed Eurasian sink of 1 GtC/year to be under estimated by 40 percent (Table 3d). These test inversions show what to expect about errors of the inverse calculations due to transport biases in a general sense, the results should not be extrapolated strictly (for instance, region by region) to inverse calculations with actual observations that resulted from real winds acting on real sources.

Table 3. Terrestrial NPP, RESP and net fluxes and oceanic uptake estimated by inverse modeling of monthly mean atmospheric CO_2 (data: NOAA CMDL network, flux unit: GtC/year, negative sign indicates flux out of the atmosphere).

(a) SKYHI model simulation of CASA net ecosystem production

Source Regions	CASA	NPP	RESP	Net	Expected
Global ocean				-0.3	0.0
Eurasia	8.9	-9.4	9.6	0.2	0.0
North America	6.2	-5.7	5.6	-0.1	0.0
Tropics & SH	33.8	-22.4	22.6	0.2	0.0

(b) SKYHI model simulation of CASA net ecosystem production + 1990 fossil fuel emissions + 1990 oceanic fluxes (Takahashi et al., 1997)

Source Regions	CASA	NPP	RESP	Net	Expected
Global ocean				-1.2	-1.1
Eurasia	8.9	-9.0	8.8	-0.2	0.0
North America	6.2	-5.6	4.9	-0.7	0.0
Tropics & SH	33.8	-22.9	24.0	1.1	0.0

(c) SKYHI model simulation of CASA net ecosystem production + a North American sink of 1 GtC/yr

Source Regions	CASA	NPP	RESP	Net	Expected
Global ocean				-0.3	0.0
Eurasia	8.9	-9.4	9.5	0.1	0.0
North America	6.2	-6.8	5.8	-1.0	-1.0
Tropics & SH	33.8	-25.6	25.7	0.1	0.0

(d) SKYHI model simulation of CASA net ecosystem production + a Eurasian sink of 1 GtC/yr

Source Regions	CASA	NPP	RESP	Net	Expected
Global ocean				-0.3	0.0
Eurasia	8.9	-10.3	9.7	-0.6	-1.0
North America	6.2	-5.8	5.7	-0.1	0.0
Tropics & SH	33.8	-21.3	21.3	0.0	0.0

The inversion results for monthly atmospheric CO_2 between 1993-1995 are shown in Table 4. The estimated annual NPP and RESP are each about 10-20 percent greater than predicted by the CASA model. Terrestrial carbon uptake was estimated for Eurasia and North America, each of size slightly over 1 GtC/year. Previously, we estimated, using an annual average inverse model, a large terrestrial uptake of carbon in North America, of about 1.5 GtC/year, between 1988-1992. A large terrestrial carbon source of 1.5-1.9 GtC/year is also estimated to be present in the region of Tropics and Southern Hemisphere. The present results are similar to that reported for the earlier period, and extend the mid-latitude Northern Hemispheric terrestrial carbon sink to a longer period of time.

Table 4. Terrestrial NPP, RESP and net fluxes estimated by inverse modeling of monthly mean atmospheric CO_2 (data: NOAA CMDL network, observations from 1993-1995, flux unit: GtC/year, negative sign indicates flux out of the atmosphere). The robust estimation method was used.

Source Regions	CASA	NPP	RESP	Net
Global ocean ^{a}				-2.2
Eurasia	8.9	-11.0	9.7	-1.3
North America	6.2	-8.3	7.2	-1.1
Tropics & SH	33.8	-0.8	2.7	1.9
Global ocean ^{b}				-2.1
Eurasia	8.9	-10.9	9.8	-1.1
North America	6.2	-8.7	7.4	-1.3
Tropics & SH	33.8	-7.5	9.0	1.5

^{a} Flux prescribed to Princeton ocean model.
^{b} Flux prescribed to Takahashi et al. (1999).

The terrestrial isotopic fluxes estimated by the inversion are shown in Table 5a for Eurasia and North America. The seasonal variations in the tropical region are so small that they do not provide sufficient information to allow a separate estimation of NPP and RESP (see Table 4). The isotopic fluxes divided by the estimated carbon fluxes give the isotopic fractionation coefficients during photosynthesis and the difference of isotopic ratios between atmospheric CO_2 and CO_2 released from soil organic matter (SOM). The estimated difference of isotopic ratios between the carbon reservoirs compares well with observations. If we assume a uniform isotopic fractionation coefficients of -20‰ for photosynthetic carbon assimilation, the isotopic fluxes can be

converted to carbon fluxes (NPP, RESP, and net, see Table 5b). The results for NPP and RESP are close to the estimates based on atmospheric CO_2 data. The atmospheric $\delta^{13}C$ data, which are independent of CO_2 measurements (although using the same air samples), appear to suggest for 1993-1995 a larger Eurasian carbon sink and a smaller North American carbon sink than implied by atmospheric CO_2 data. Year-by-year analysis indicates data from 1994 to be mostly responsible for the discrepancy (results not shown here). We will identify stations that "saw" the difference.

The isotopic fractionation coefficients vary significantly from boreal forest to temperate forest and to tropical savanna (Neil Suits, Colorado State University, personal communication). However, we did not have the terrestrial model results when the isotopic inverse model was constructed; we assumed uniform isotopic fractionations for the three large regions.

The modeled CO_2 mixing ratios and $\delta^{13}C$ values are compared to observations in Figure 5 for selected stations from north to south. At Barrow, Alaska, and Bermuda Island, the model lags the observation in the fall in CO_2 growth and in $\delta^{13}C$ decrease, while the seasonal amplitudes are in good agreement. By contrast, the model leads the observation by a month at Key Biscayne, Florida. Large residuals result from a mismatch of the seasonal phase between model and observation at many stations. At some stations in the North Pacific (Guam Island, Kumukahi, and Mauna Loa) the model underpredicts the seasonal amplitude, while at other stations (Midway, Shemya) the model agrees well with the observations. At stations located in the Southern Hemisphere (Samoa, South Pole), the model captures the long-term trend, but does not agree well in seasonal variability, although the seasonal fluctuations are small in the Southern Hemisphere. It appears that the dis-equilibrium isotopic fluxes in the Southern Ocean was over-estimated, causing a greater than observed decrease of atmospheric $\delta^{13}C$ at the South Pole, where the agreement is good for atmospheric CO_2 mixing ratio. As land biomes are small in size in the extra-tropical Southern Hemisphere, seasonal changes in ocean biology and sea surface temperature can cause

atmospheric CO_2 and $\delta^{13}C$ variations comparable in size to that due to terrestrial ecosystems.

Table 5a. Terrestrial NPP and RESP fluxes estimated by inverse modeling of monthly mean atmospheric CO_2 and $\delta^{13}C$ of CO_2 (data: NOAA CMDL network, observations from 1993-1995, negative sign indicates flux out of the atmosphere)

Source Regions	Flux	GtC/yr	‰GtC/yr	ε (‰)
Eurasia	NPP	-11.0	220.0	-20.0
	RESP	9.7	-188.0	-19.4
North America	NPP	-8.3	161.7	-19.5
	RESP	7.2	-148.0	-20.6

Note: Oceanic fluxes of CO_2 and $^{13}CO_2$ were prescribed according to the Princeton ocean biogeochemistry model.

Table 5b. Terrestrial NPP and RESP fluxes estimated by inverse modeling of monthly mean atmospheric CO_2 and $\delta^{13}C$ of CO_2 (data: NOAA CMDL network, observations from 1993-1995, negative sign indicates flux out of the atmosphere)

Source Regions	Flux	‰GtC/yr	GtC/yr #
Eurasia	NPP	220.0	-11.0
	RESP	-188.0	9.4
	Net	32.0	-1.6
North America	NPP	161.7	-8.1
	RESP	-148.0	7.4
	Net	13.7	-0.7

Note: Oceanic fluxes of CO_2 and $^{13}CO_2$ were prescribed according to the Princeton ocean biogeochemistry model. #Assume ε = -20‰ and assume there is no disequilibrium between soil respired CO_2 and the atmosphere.

Our prescribed ocean fluxes are based on annual average ocean model results, and therefore do not have seasonal variations. Furthermore, we did not consider interannual variabilities in our inverse model. The model and data comparison can be improved by fitting to data one year at a time, and using ocean fluxes with a seasonal resolution.

4. Future Work

There are two areas for improvement in the inverse model. First, we need accurate and seasonally resolved oceanic fluxes of carbon isotopes. Synthesis of ocean measurements obtained during JGOFS and WOCE programs will provide new observational constraints on the air-sea exchange. New ocean biogeochemistry models are under development that use improved ocean circulation and ocean biology. Secondly, we need realistic representation of the spatial and temporal variations of terrestrial carbon isotopes fluxes. A new terrestrial biogeochemistry model of carbon cycle is under development at Colorado State University, and will provide improved terrestrial "basis functions" for our inverse model.

Acknowledgments: We thank Bob Andres (University of Alaska Fairbanks) for producing the monthly isotopic ratios maps for the US fossil fuel carbon emissions and annual maps for the world. The observations of atmospheric CO_2 and $\delta^{13}C$ ratio of CO_2 were made by the NOAA CMDL (directed by Pieter Tans) in colaboration with the INSTARR University of Colorado (directed by Jim White). Computational resource and the atmospheric transport models were provided to us by GFDL, courtesy of Jerry Mahlman.

References

Andres, R.J., G. Marland, I. Fung, and E. Matthews, A 1° x 1° distribution of carbon dioxide emissions from fossil fuel consumption and cement manufacture, 1950-1990, *Global Biogeochemical Cycles, 10*, 419-429, 1995.

Fan, S., M. Gloor, J. Mahlman, S. Pacala, J. Sarmiento, T. Takahashi, and P. Tans, A large terrestrial carbon sink in North America implied by atmospheric and oceanic CO_2 data and models, *Science, 282*, 442-446, 1998.

Gloor, M., S.-M. Fan, S.W. Pacala, J. L. Sarmiento, and M. Ramonet, A model-based evaluation of inversions based on atmospheric transport, using annual mean mixing ratios, as a tool to monitor fluxes of nonreactive trace substances like CO2 on a continental scale, *Journal of Geophysical Research, 104*, 14,245-14,260, 1999.

Gloor, M., S.-M. Fan, S.W. Pacala, and J. L. Sarmiento, Optimal sampling of the atmosphere for purpose of inverse modeling - a model study, *Global biogeochemical Cycles, 14*, 407-428, 2000.

Murnane, R.J., and J.L. Sarmiento, Roles of biology and gas exchange in determining the $\delta^{13}C$ distribution in the ocean and the preindustrial gradient in atmospheric $\delta^{13}C$, *Global biogeochemical Cycles, 14*, 389-405, 2000.

Murnane, R.J., J.L. Sarmiento, and C. Le Quere, Spatial distribution of air-sea CO_2 fluxes and the interhemispheric transport of carbon by the oceans, *Global Biogeochemical Cycles, 13*, 287-305, 1999

Potter, C.S., et al., Terrestrial ecosystem production: A process model based on global satellite and surface data, *Global biogeochemical Cycles, 7*, 811-841, 1993.

Press, W.H., S.A. Teukolsky, W.T. Vetterling, and B.P. Flannery, *Numerical Recipes in C, The Art of Scientific Computing*, second edition, Cambridge University Press, 1992.

Takahashi, T., R.A. Feely, R. Weiss, R.H. Wanninkhof, D.W. Chipman, S.C. Sutherland, and T. Takahashi, Global air-sea flux of CO_2: An estimate based on measurements of sea-air pCO_2 difference, *Proceedings of the National Academy of Sciences, U.S.A., 94*, 8292-8299, 1997.

Tans, P.P. I.Y. Fung, and T. Takahashi, Observational constraints on the global atmospheric CO2 budget, *Science, 247*, 1431-1438, 1990.

Figure Captions

Figure 1. A world map of carbon isotopic ratios of fossil CO_2 released by each nation.

Figure 2. A U.S. map of isotopic ratios of fossil CO_2 released by each state in 1995. (a) January, (b) July.

Figure 3. A map of terrestrial source regions defined for the inverse model.

Figure 4. Zonal average $\delta^{13}C$ caused by fossil emissions and oceanic fluxes, shown as deviations from January value at the Sout Pole Observatory.

Figure 5. Comparison of observations and post-inversion model predictions at selected stations.

Fig. 1

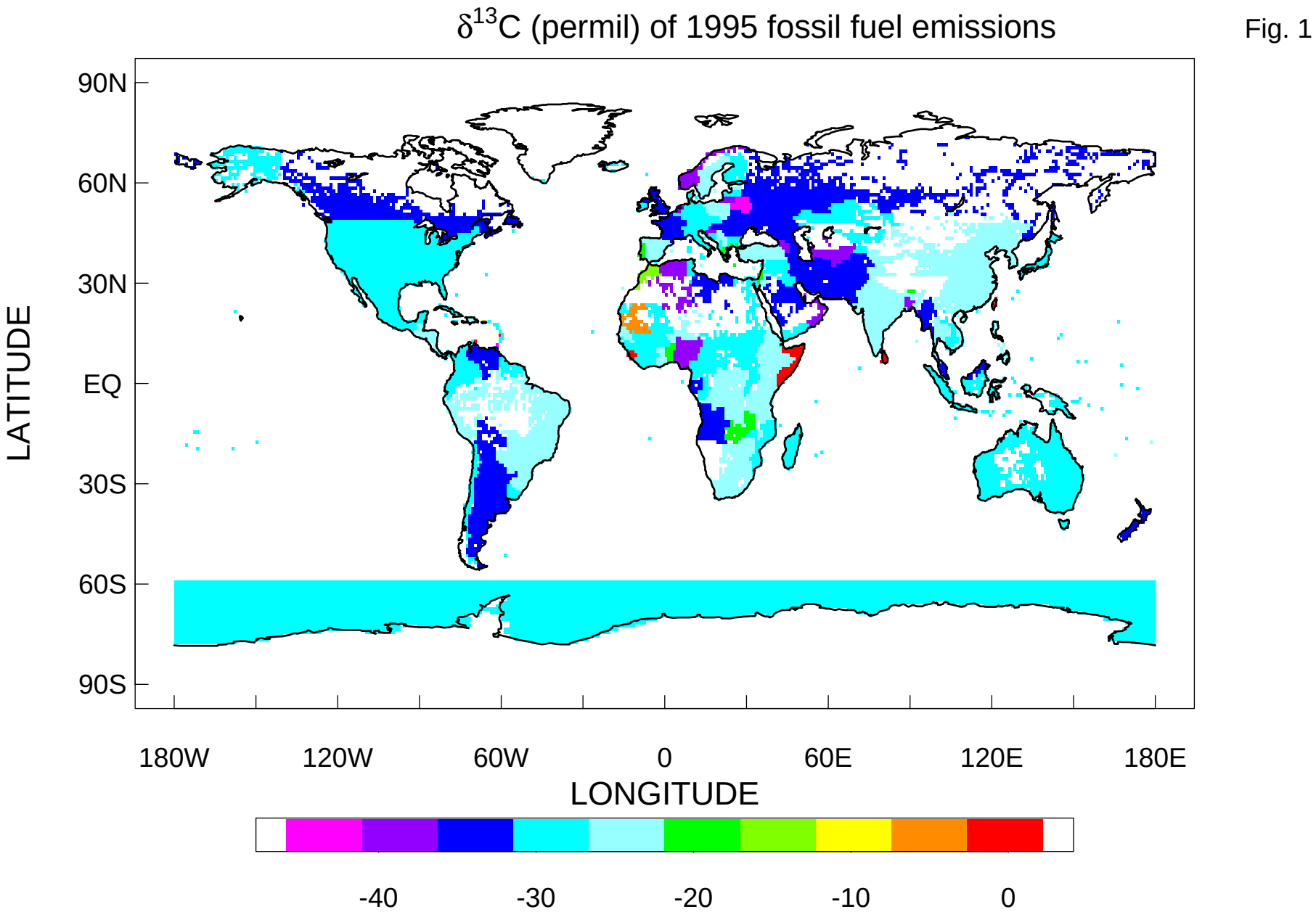
δ13C (permil) of 1995 fossil fuel emissions
90N
60N
30N
EQ
30S
60S
90S
LATITUDE
180W
120W
60W
0
60E
120E
180E
LONGITUDE
-40
-30
-20
-10
0

Fig. 2a

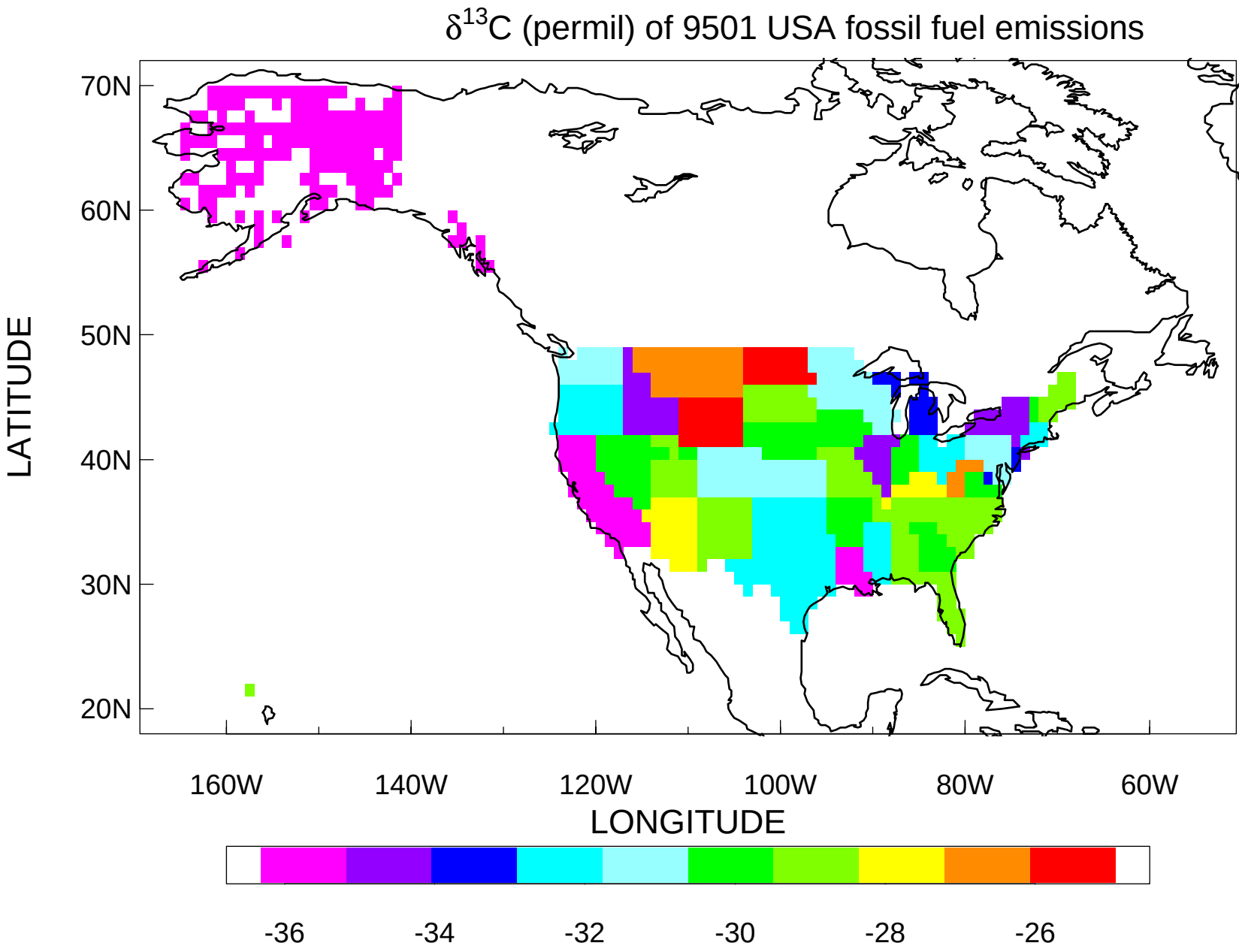
δ13C (permil) of 9501 USA fossil fuel emissions
70N
60N
50N
40N
30N
20N
LATITUDE
160W
140W
120W
100W
80W
60W
LONGITUDE
-36
-34
-32
-30
-28
-26

Fig. 2b

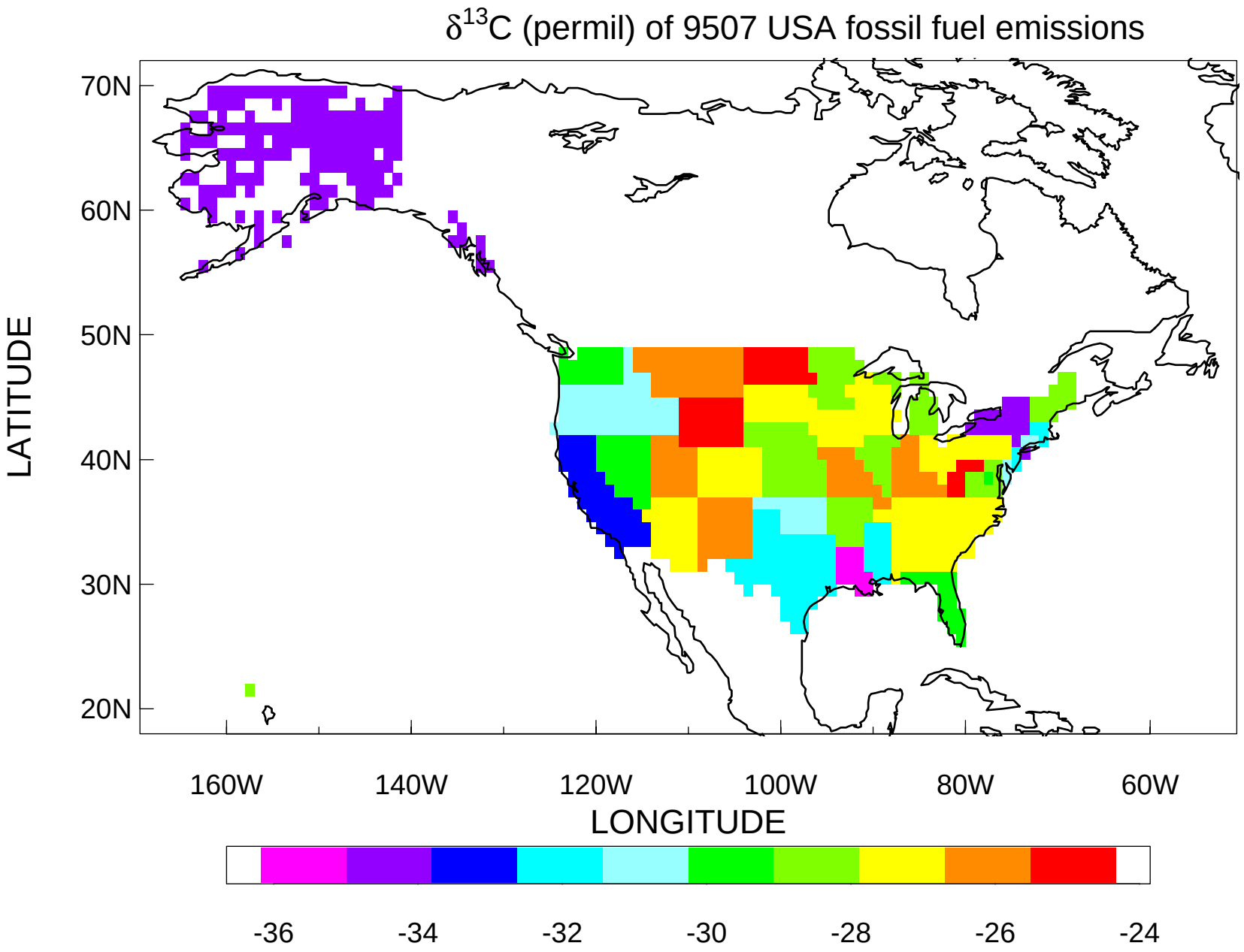
δ13C (permil) of 9507 USA fossil fuel emissions
70N
60N
50N
40N
30N
20N
LATITUDE
160W
140W
120W
100W
80W
60W
LONGITUDE
-36
-34
-32
-30
-28
-26
-24

Fig. 3

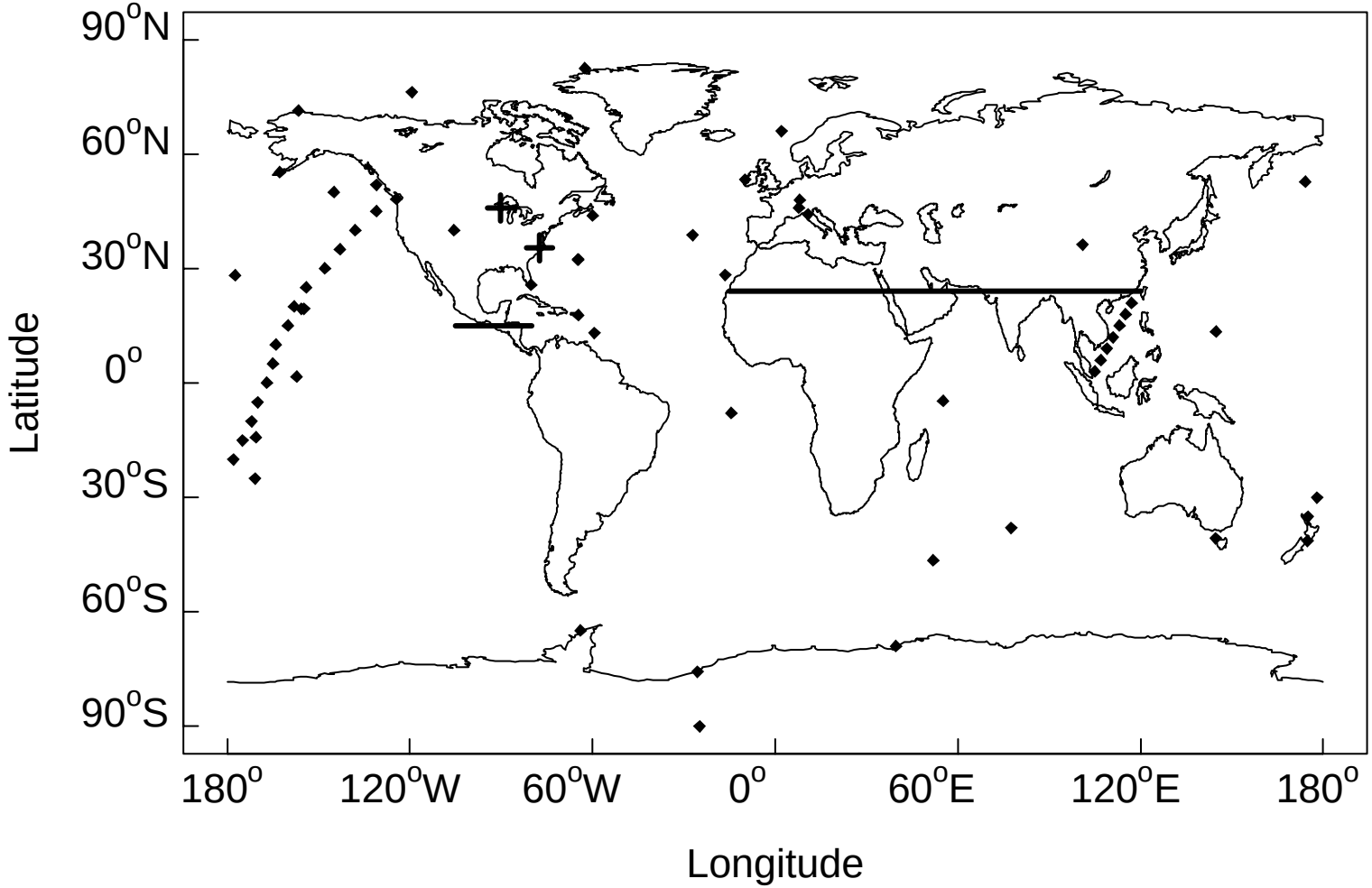
90°N
60°N
30°N
0°
30°S
60°S
90°S
Latitude
180°
120°W
60°W
0°
60°E
120°E
180°
Longitude

Annual Zonal Mean in Atmopsheric Surface Layer

Fig. 4

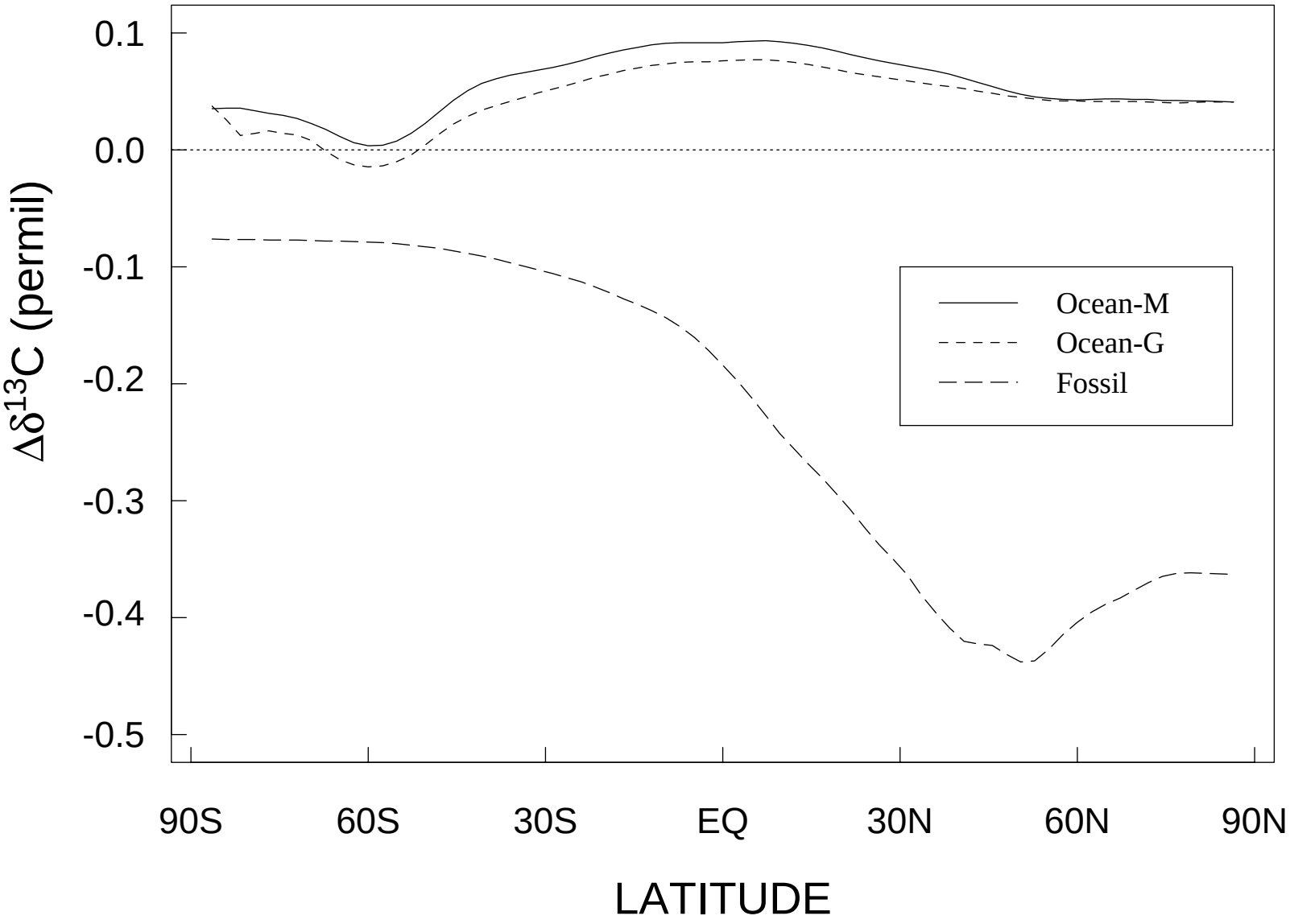

Fig. 5a

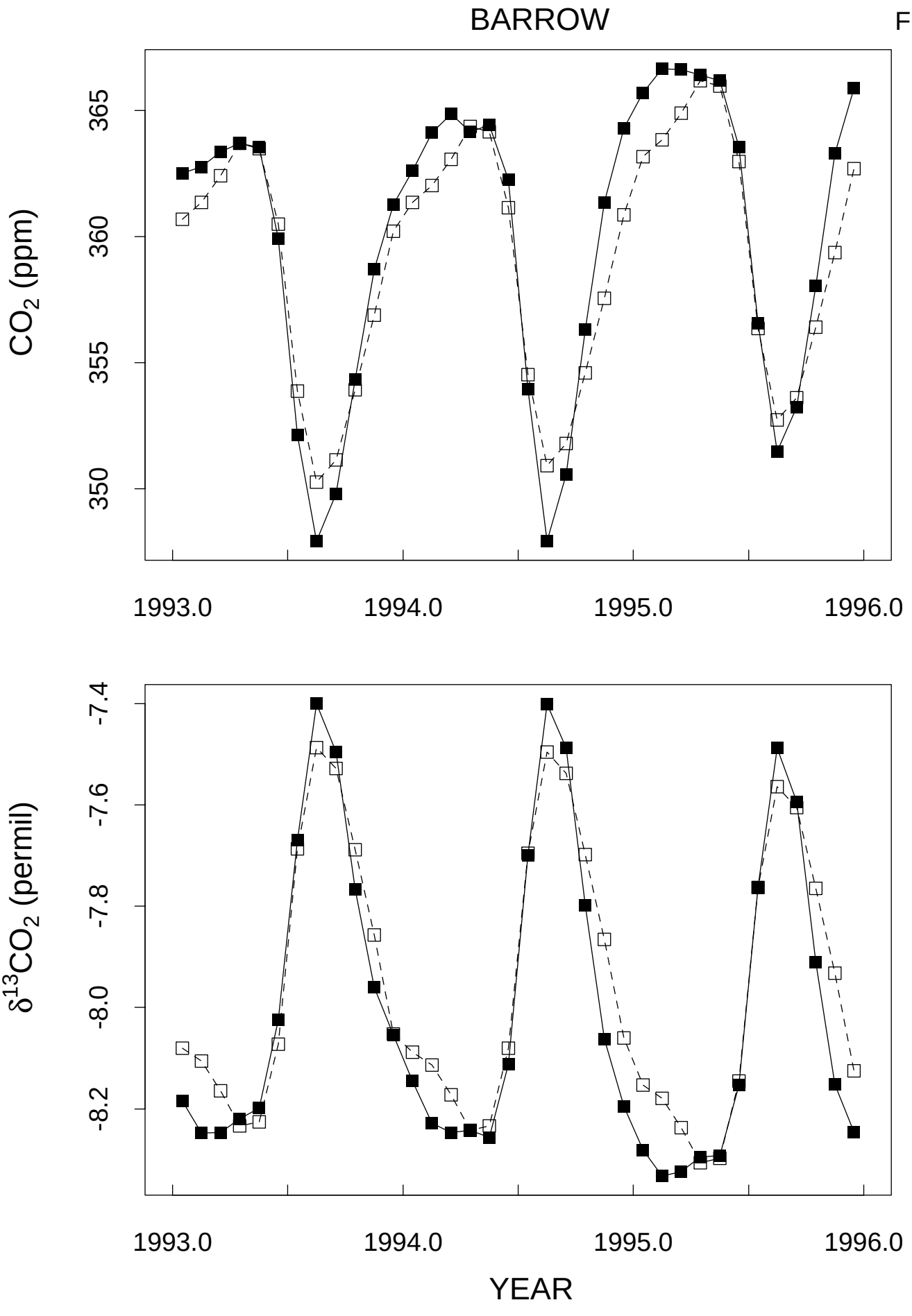
BARROW
CO2 (ppm)
365
360
355
350
1993.0
1994.0
1995.0
1996.0
δ13CO2 (permil)
-7.4
-7.6
-7.8
-8.0
-8.2
1993.0
1994.0
1995.0
1996.0
YEAR

Fig. 5b

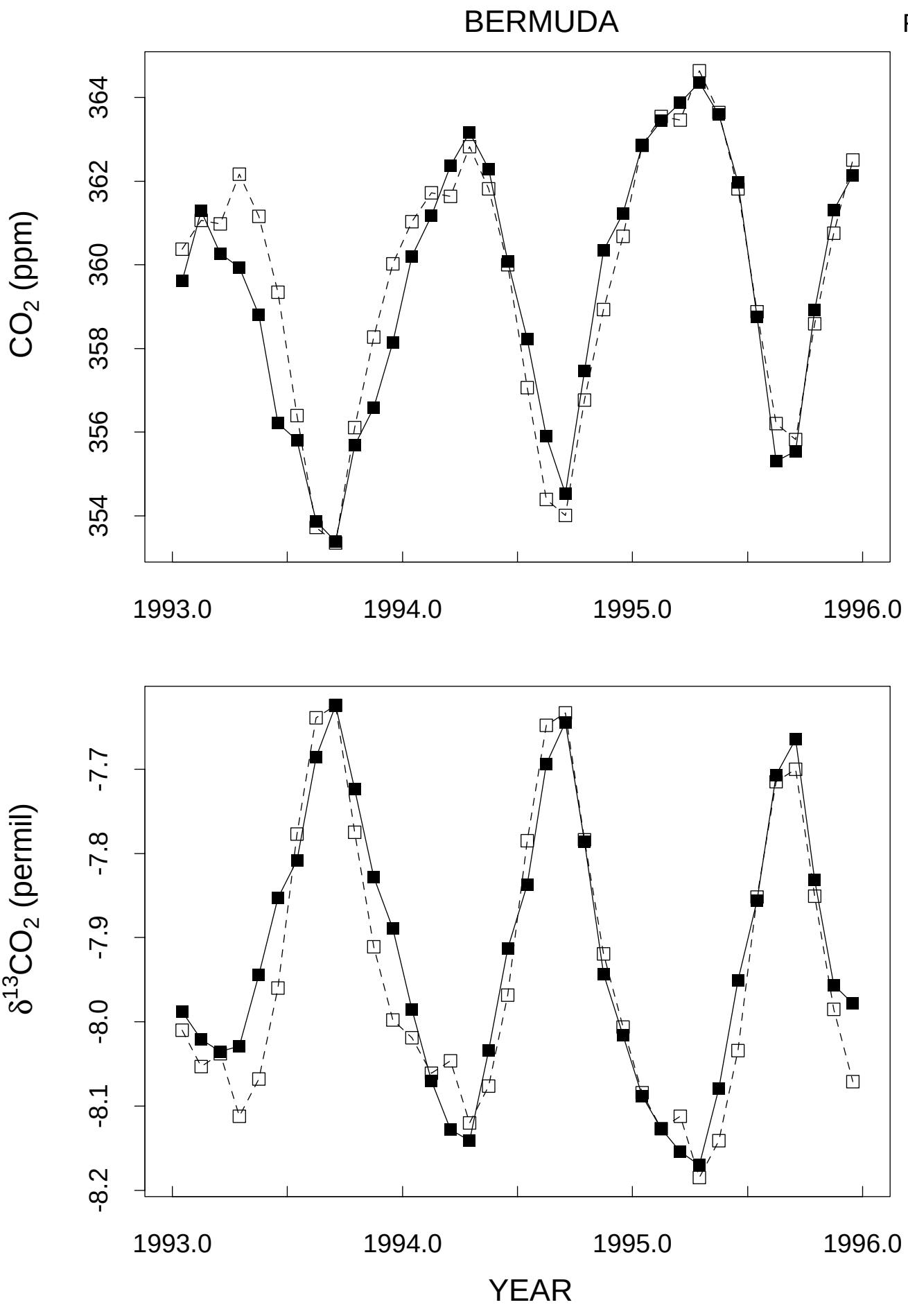
BERMUDA
CO_2 (ppm)
364
362
360
358
356
354
1993.0
1994.0
1995.0
1996.0
$\delta^{13}CO_2$ (permil)
-7.7
-7.8
-7.9
-8.0
-8.1
-8.2
1993.0
1994.0
1995.0
1996.0
YEAR

KEY BISCAYNE

Fig. 5c

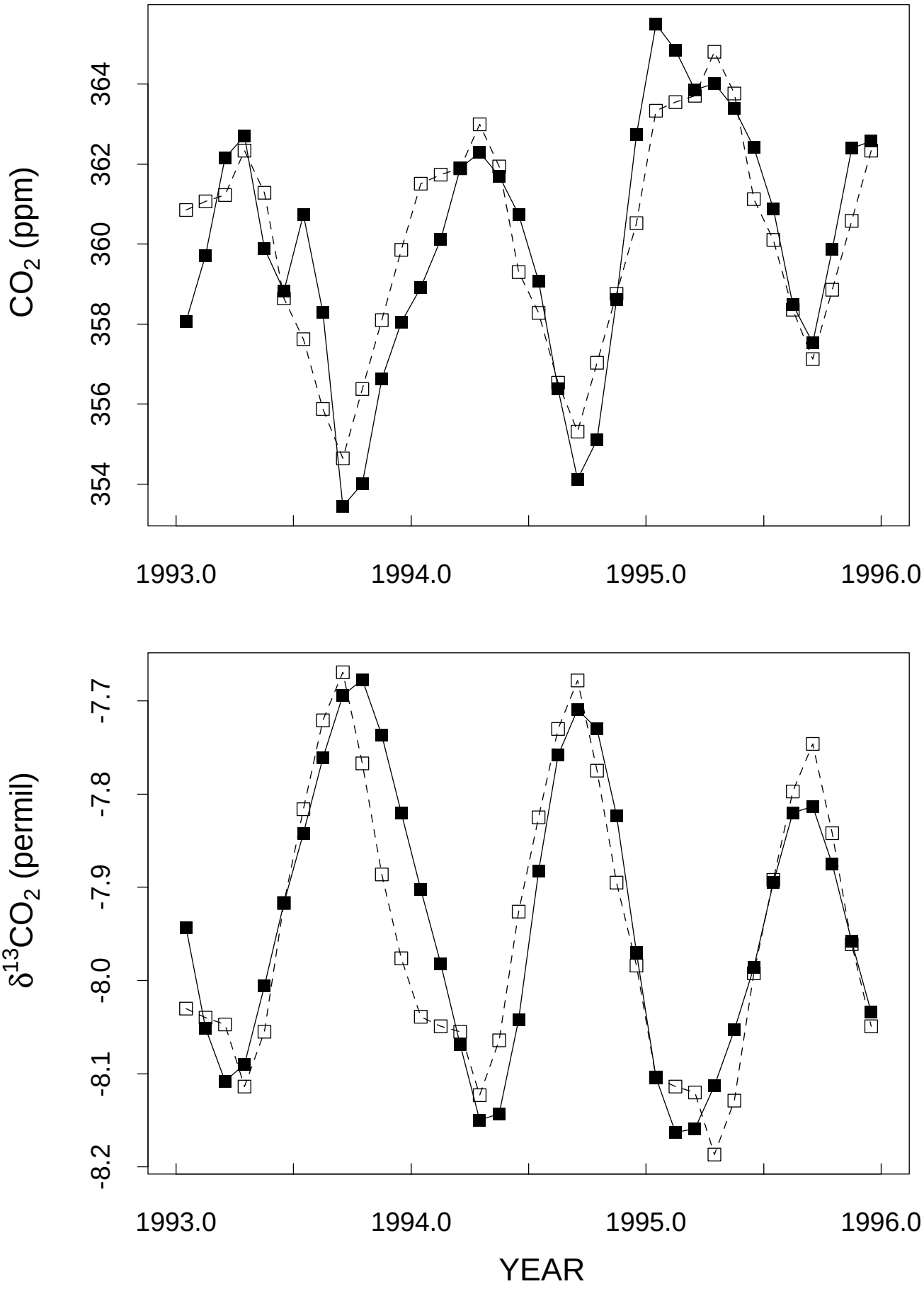

GUAM ISLAND

Fig. 5d

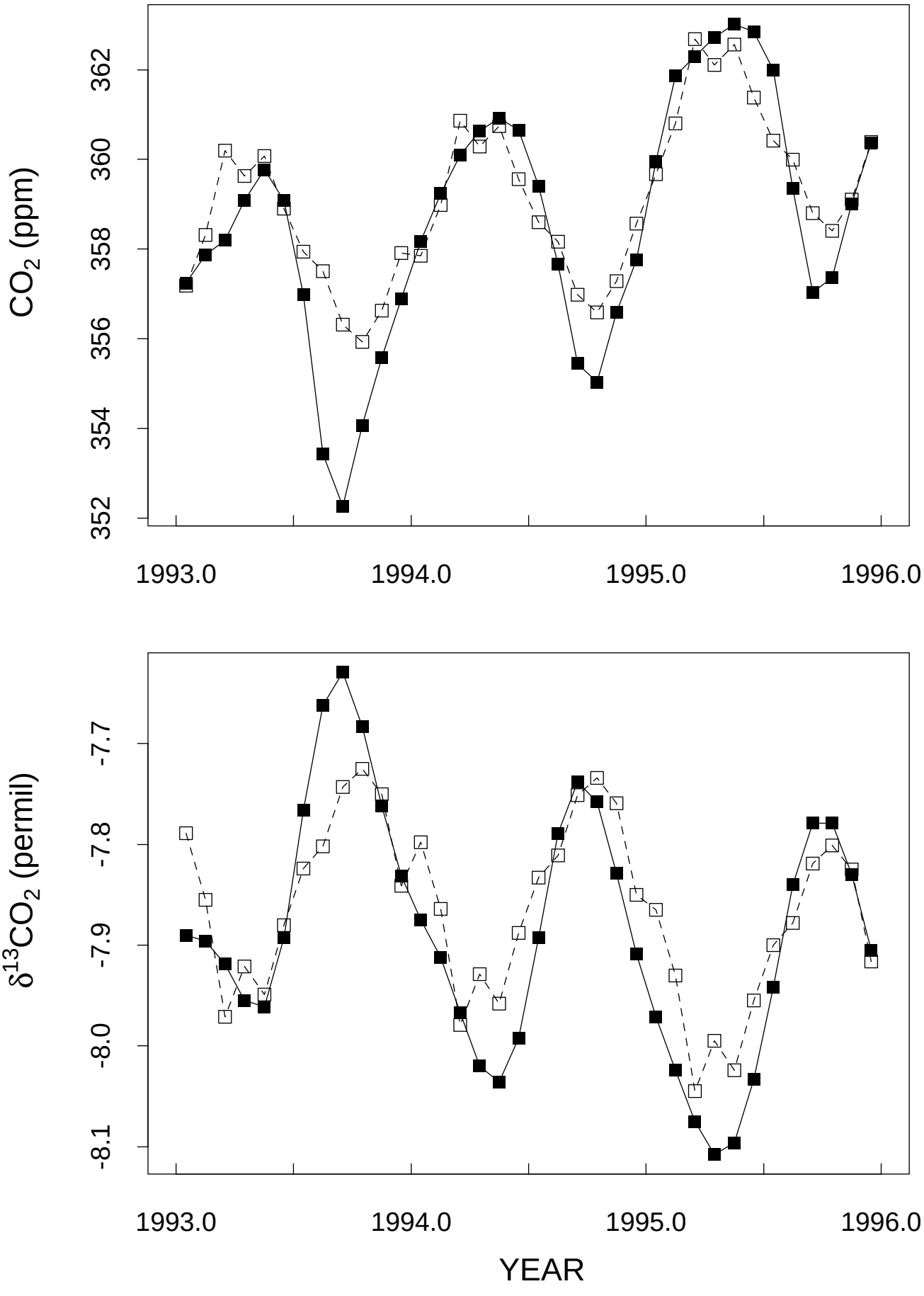

KUMUKAHI

Fig. 5e

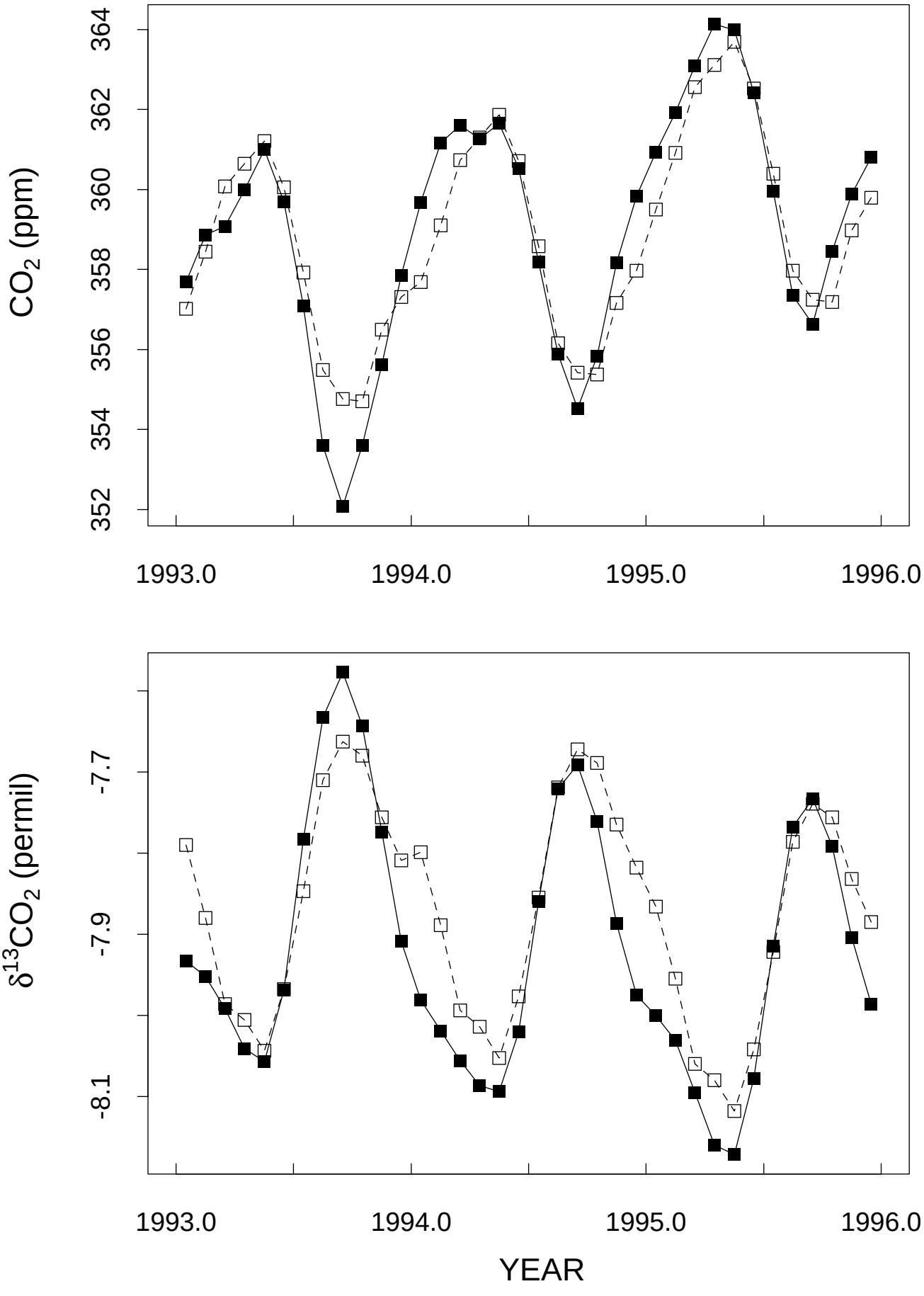

Fig. 5f

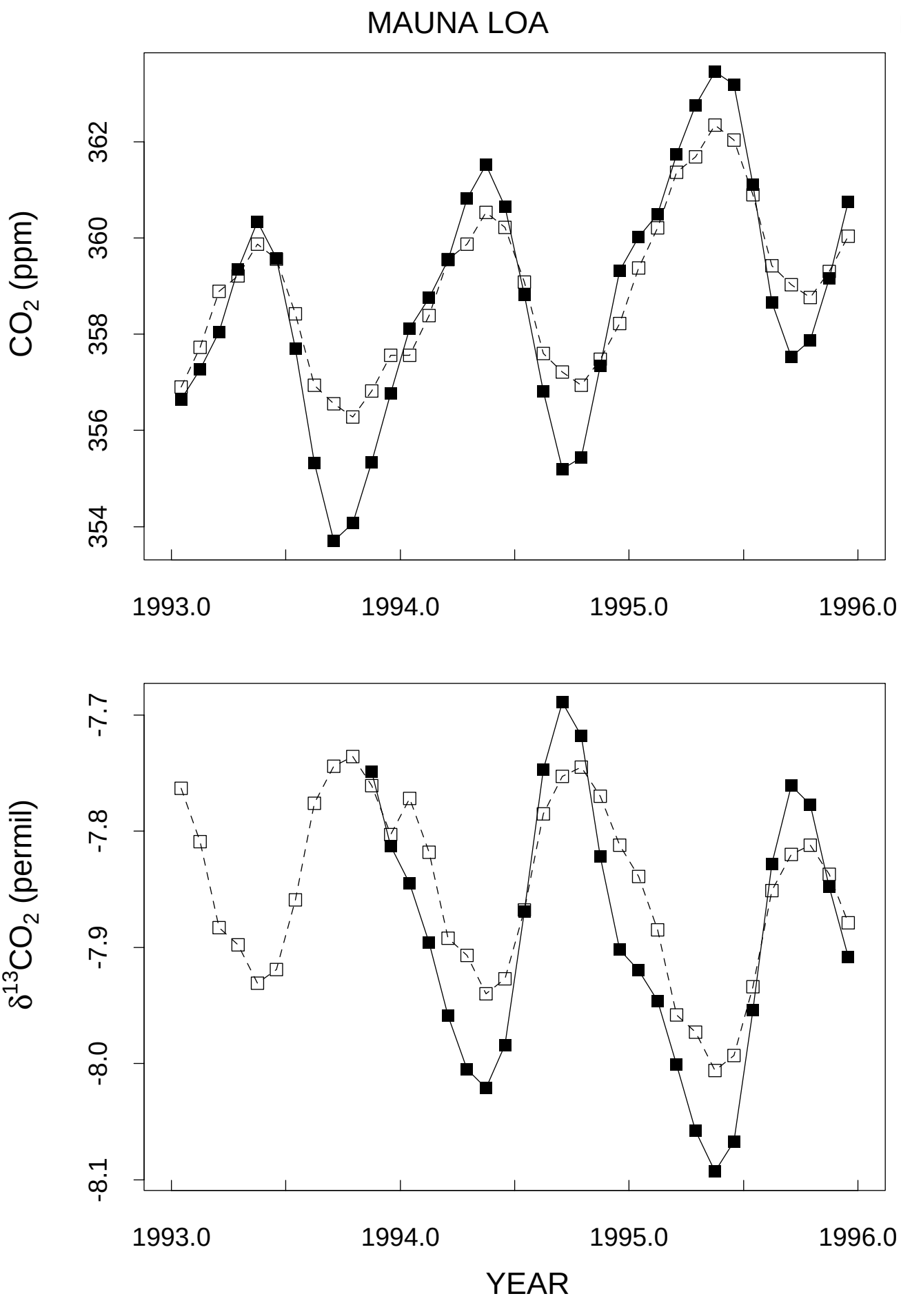
MAUNA LOA
CO2 (ppm)
354
356
358
360
362
δ13CO2 (permil)
-8.1
-8.0
-7.9
-7.8
-7.7
1993.0
1994.0
1995.0
1996.0
YEAR

Fig. 5g

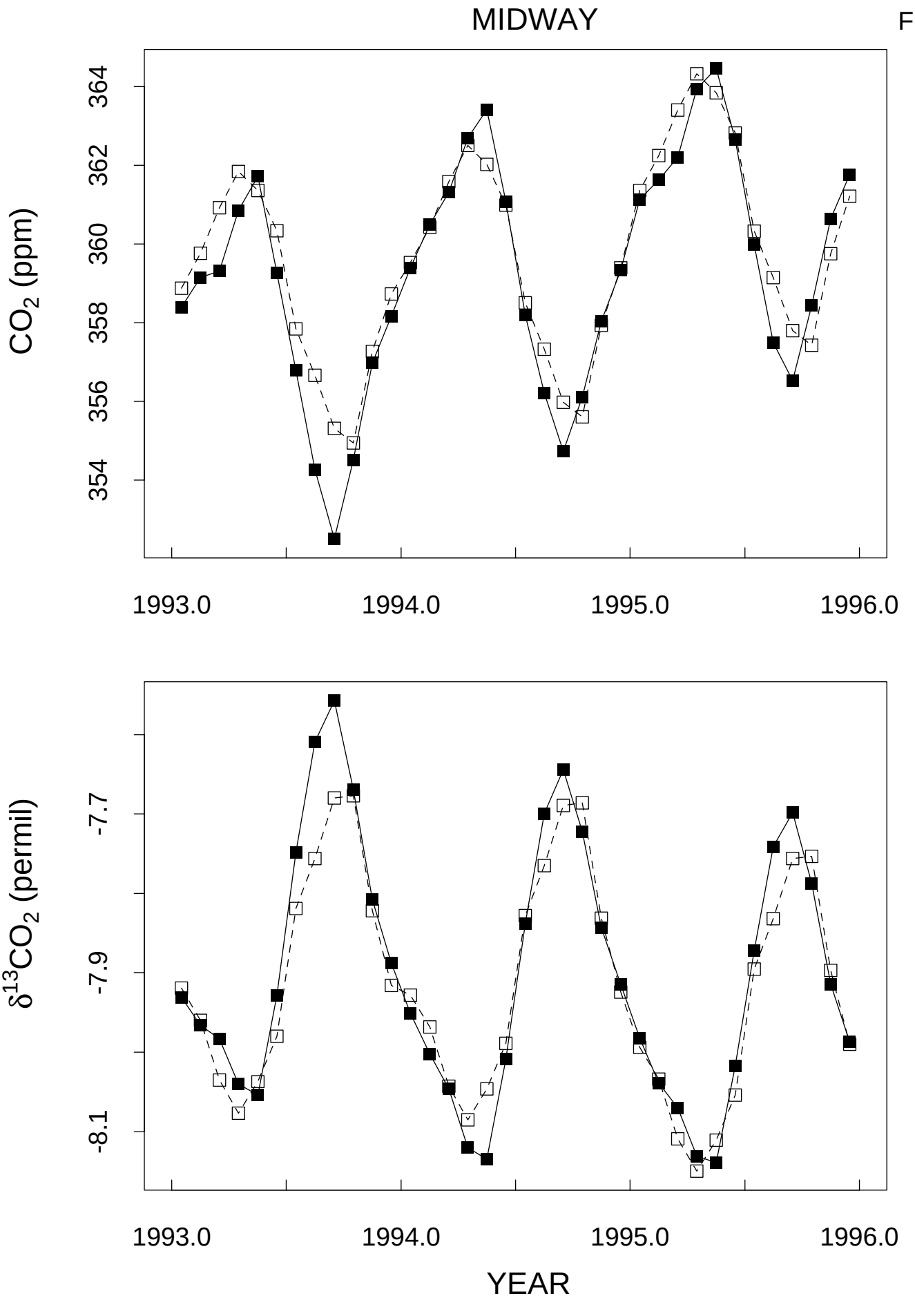
MIDWAY
CO_2 (ppm)
364
362
360
358
356
354
1993.0
1994.0
1995.0
1996.0
$\delta^{13}CO_2$ (permil)
-7.7
-7.9
-8.1
1993.0
1994.0
1995.0
1996.0
YEAR

SHEMYA

Fig. 5h

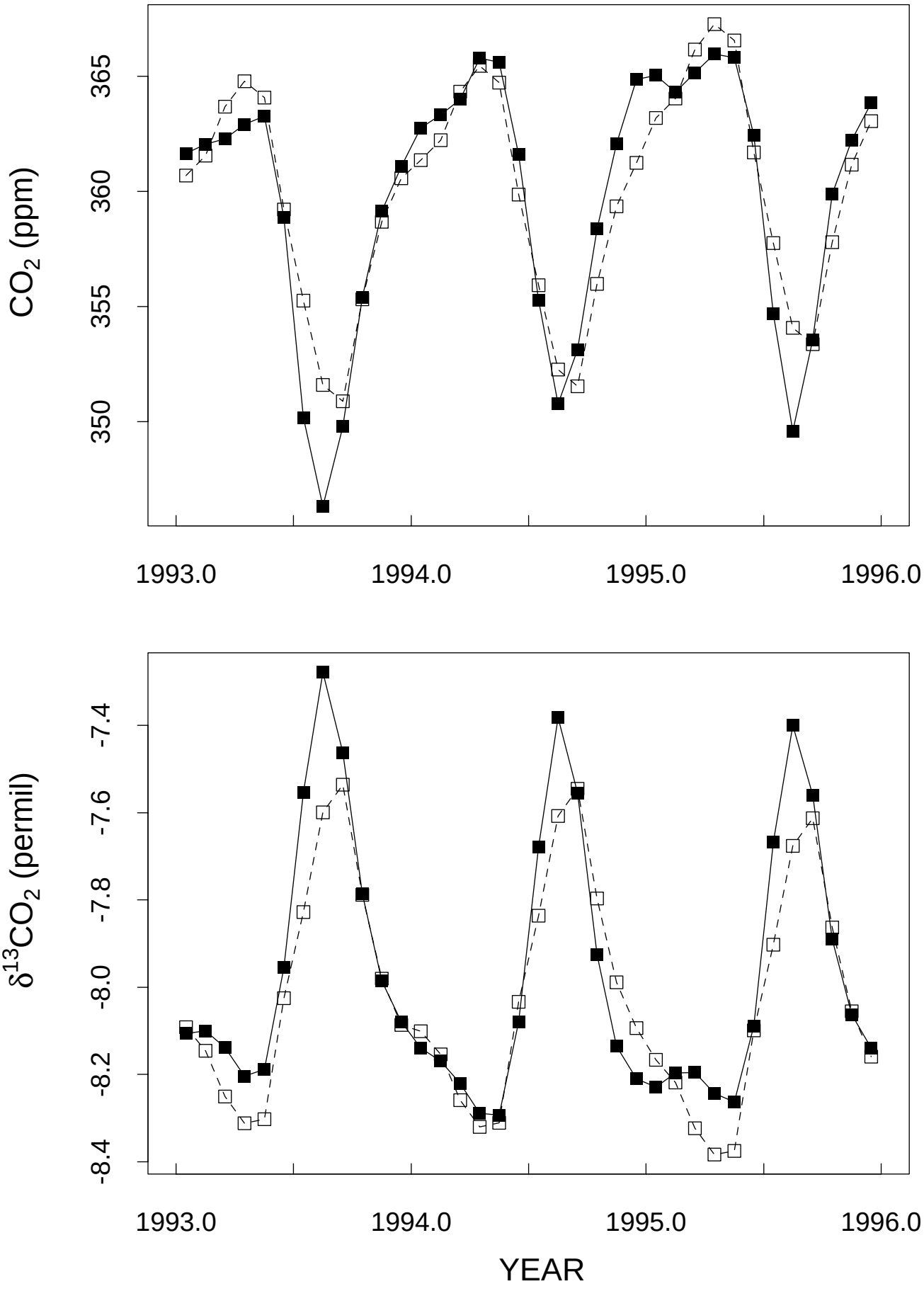

Fig. 5i

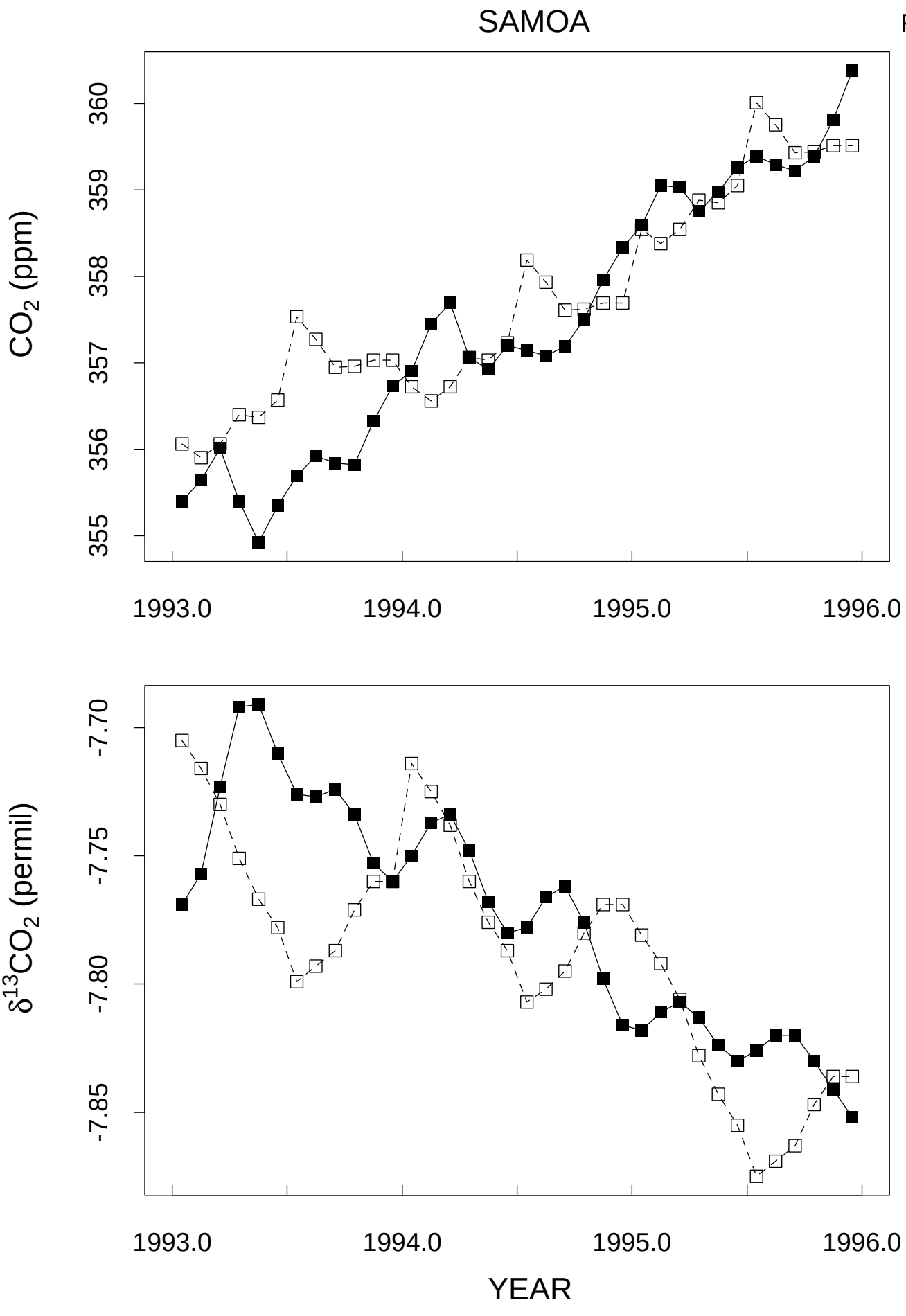
SAMOA
CO_2 (ppm)
355
356
357
358
359
360
1993.0
1994.0
1995.0
1996.0
$\delta^{13}CO_2$ (permil)
-7.85
-7.80
-7.75
-7.70
1993.0
1994.0
1995.0
1996.0
YEAR

Fig. 5j

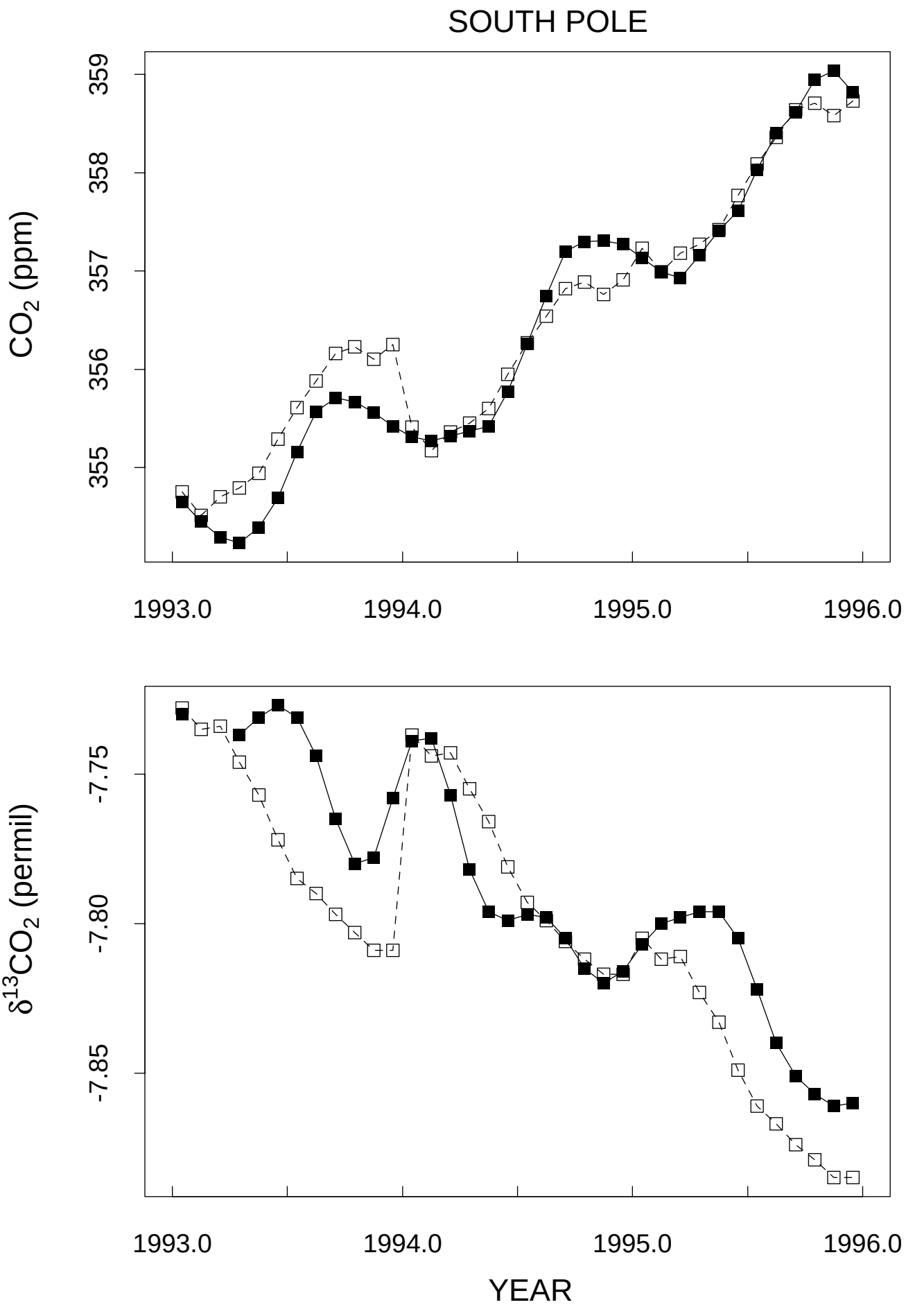
SOUTH POLE
CO2 (ppm)
359
358
357
356
355
1993.0
1994.0
1995.0
1996.0
δ13CO2 (permil)
-7.75
-7.80
-7.85
1993.0
1994.0
1995.0
1996.0
YEAR